SCIENCE CHINA
Physics, Mechanics & Astronomy

• Article •

July 2017 Vol. 60 No. 7: 070311
doi: 10.1007/s11433-017-9039-0

Second-order magnetic field gradient-induced strong coupling between nitrogen-vacancy centers and a mechanical oscillator

Kang Cai[1], RuiXia Wang[1], ZhangQi Yin[2*], and GuiLu Long[1,3,4*]

[1] *State Key Laboratory of Low-Dimensional Quantum Physics and Department of Physics, Tsinghua University, Beijing 100084, China;*
[2] *Center for Quantum Information, Institute for Interdisciplinary Information Sciences, Tsinghua University, Beijing 100084, China;*
[3] *Tsinghua National Laboratory of Information Science and Technology, Beijing 100084, China;*
[4] *Collaborative Innovation Center of Quantum Matter, Beijing 100084, China*

Received March 17, 2017; accepted April 12, 2017; published online April 27, 2017

We consider a cantilever mechanical oscillator (MO) made of diamond. A nitrogen-vacancy (NV) center lies at the end of the cantilever. Two magnetic tips near the NV center induce a strong second-order magnetic field gradient. Under coherent driving of the MO, we find that the coupling between the MO and the NV center is greatly enhanced. We studied how to generate entanglement between the MO and the NV center and realize quantum state transfer between them. We also propose a scheme to generate two-mode squeezing between different MO modes by coupling them to the same NV center. The decoherence and dissipation effects for both the MO and the NV center are numerically calculated using the present parameter values of the experimental configuration. We have achieved high fidelity for entanglement generation, quantum state transfer, and large two-mode squeezing.

second-order magnetic field gradient, NV center, mechanical oscillator, entanglement, state transfer, squeezing

PACS number(s): 07.10.Cm, 03.67.Mn, 02.60.Jh, 42.50.Ar, 42.50.Pq

Citation: K. Cai, R. X. Wang, Z. Q. Yin, and G. L. Long, Second-order magnetic field gradient-induced strong coupling between nitrogen-vacancy centers and a mechanical oscillator, Sci. China-Phys. Mech. Astron. **60**, 070311 (2017), doi: 10.1007/s11433-017-9039-0

Because of its applications in ultra-high precise sensing and testing quantum phenomenon at macroscopic scale [1,2], the nano(micro)-mechanical oscillator has attracted much attention in recent years. Combined with cavity opto- and electromechanics, the mechanical oscillator (MO) has been explored extensively as a quantum interface [3-11]. Moreover, strong coupling in hybrid MO systems have been realized that may be used to achieve for example ground-state cooling and quantum information processing [12-15]. Recently, the focus has been on interfacing the mechanical degrees of freedom with a single quantum object such as a 2-level system with a quantum state that can be precisely controlled. One such system investigated both theoretically and experimentally couples a nanomechanical oscillator with solid state qubits, such as nitrogen-vacancy (NV) centers in diamond [16-27].

Resonating nanostructures made of a single-crystal diamond are expected to possess excellent mechanical properties, including high quality factors and low dissipation. Diamond has been expected to have great applications as a uniquely versatile material, albeit one that is intricate to grow and process. Fortunately, values for the quality factors exceeding one million are found at room temperature that surpass those of single-crystal silicon cantilevers of similar dimensions by roughly an order of magnitude [28]. In addition, diamond hosts interesting intrinsic dopants [29]—The most prominent are the NV centers. Each NV center is formed by a nitrogen atom and a nearby vacancy in diamond, negatively charged and usually possessing six electrons in a ground state

*Corresponding authors (ZhangQi Yin, email: yinzhangqi@tsinghua.edu.cn; GuiLu Long, email: gllong@tsinghua.edu.cn)

with spin $S = 1$. The centers are regarded as artificial atoms in the solid system [30]. Because of the long coherence time and sensitive to magnetic field, they are viewed as units for quantum information processing and also widely used as solid-state ultra-sensitive magnetic field sensors.

There are usually two methods to couple the NV centers with a MO. The first requires a strain-induced effective electric field to mix phonon modes with the electron spin of the NV centers [31-34]. Strain-induced coupling is very sensitive to the size of the MO. The strong coupling regime is very difficult to approach from such a direction. The second method is based on the strong first-order magnetic field gradient [17, 35]. For this method, one of the main problems with the hybrid systems of a NV center and a MO is the strong coupling condition requiring an ultra-high magnetic gradient [17]. One solution is to reduce the effective mass of the oscillator or trapping frequency [36, 37]. Here we study the third coupling mechanism between a NV center and MO based on second-order magnetic coupling, which was studied in heating one mode of a MO to cool another mode to the quantum ground regime [38]. The advantage of this mechanism is that the effective coupling strength between mechanical mode and electrons spins can be easily tuned.

In this article, we propose a scheme to realize strong coupling between a MO and a NV center under the second-order magnetic field gradient. In sect. 1, we introduce a new model used to describe this coupling and demonstrate the increased coupling between them. In sect. 2, we propose a scheme to generate entanglement and to realize state transfer between the NV center and the MO. Then we generalize our model to the interaction between the MO and the ensemble of NV centers. In sect. 3, we present another application of two-mode squeezing for the MO. In sect. 4, we give a brief discussion and summary.

1 Model

A nano-diamond MO (Figure 1) was fabricated with a NV center situated at the end of the oscillator that oscillates vertically (x axis) in a magnetic field generated by two magnetic tips point situated symmetrically on the two sides of oscillator [38]. The MO has two modes with frequencies denoted by ω_a and ω_b. The symmetrical arrangement of tips provides a vanishing first-order magnetic field gradient near the NV center; that is, there is only a second-order magnetic field gradient. An external static magnetic field B_{ext} is present along the axial direction of the MO (z axis). The frequency difference between the electron spin states of the NV center $|-1\rangle$ and $|0\rangle$ is denoted as ω_z, where we assume that the axes of the NV center is the same as external coordinate. We establish $|0\rangle$ as

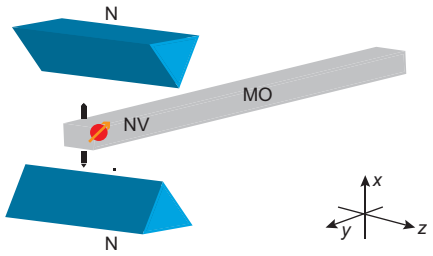

Figure 1 (Color online) Model for second-order magnetic field gradient coupling between a NV center and a diamond MO. NV centers are located at the end of the MO. Two magnetic tips are symmetrically placed either side of the MO to produce a second-order magnetic field gradient near the NV centers. Under external driving, the MO oscillates along the x direction. The homogeneous external magnetic field is along the z direction.

the ground state $|g\rangle$ and $|-1\rangle$ as the excited $|e\rangle$. The driving force is exerted on the oscillator with frequency ω_a. The energy split of the NV center electron spin is tuned to satisfy the relation $\omega_z = \omega_b - \omega_a = \Delta$. In the rotating frame $H_{10} = \omega_a a^\dagger a + \omega_a b^\dagger b$, the two-mode Hamiltonian simplifies to [38, 39]

$$\begin{aligned} H_0 &= \frac{\omega_z}{2}\sigma_z + \triangle b^\dagger b + \frac{\Omega_1}{2}\left(a + a^\dagger\right) + \frac{\Omega_2}{2}\left(b + b^\dagger\right), \\ H_1 &= \left[g_a a^\dagger a + g_b b^\dagger b + g_{ab}\left(a^\dagger b + b^\dagger a\right)\right]\sigma_x, \end{aligned} \tag{1}$$

where $a\left(a^\dagger\right)$ and $b\left(b^\dagger\right)$ represent the annihilation (creation) operators of the two oscillator phonon modes, and Ω_1 (Ω_2) is the driving strength for the mode a (b); g_a, g_b, and g_{ab} are the coupling strengths for the second-order magnetic field gradient. The Pauli operators are defined as $\sigma_z = |e\rangle\langle e| - |g\rangle\langle g|$, $\sigma_x = |e\rangle\langle g| + |g\rangle\langle e|$. With the symmetrical magnetic tip arrangement, the first-order coupling interaction between the NV center and the MO vanishes and the second-order interaction governs the system, which is described by term H_1.

Initially, the magnetic field is absent and only the uncoupled Hamiltonian term H_0 matters. In the presence of a driving force, the MO tends to behave coherently. The dynamics of the MO can be derived from the quantum Langevin equation [40]

$$\begin{aligned} \dot{a} &= -\mathrm{i}\,[a, H_0] - \frac{\gamma_1}{2}a + \sqrt{\gamma_1}a_{\text{in}}, \\ \dot{b} &= -\mathrm{i}\,[b, H_0] - \frac{\gamma_2}{2}b + \sqrt{\gamma_2}b_{\text{in}}, \end{aligned} \tag{2}$$

where γ_1 and γ_2 are the dissipation rates of modes a and b, and a_{in} and b_{in} are the input noise operators for modes a and b, with $\langle a_{\text{in}}\rangle = \langle b_{\text{in}}\rangle = 0$. The steady state amplitude of each mode satisfies

$$\begin{aligned} &\mathrm{i}\frac{\Omega_1}{2} + \frac{\gamma_1}{2}\alpha = 0, \\ &\mathrm{i}\triangle\beta + \mathrm{i}\frac{\Omega_2}{2} + \frac{\gamma_2}{2}\beta = 0, \end{aligned} \tag{3}$$

where $\alpha = -\mathrm{i}\Omega_1/\gamma_1$ and $\beta = -\Omega_2/2\Delta$. In practice, we assume $\Omega_2 \ll \Delta$. Therefore, β approaches zero and can be neglected.

We see that by increasing the amplitude of the phonon mode, the effective coupling strength between the NV center and the MO increases. Once the steady state is established, we turn the magnetic field on and the second-order interaction between the NV center and the MO comes into effect. Near the steady state, we make the transformation $a \to a + \alpha$ and $b \to b + \beta$ under which the Hamiltonian takes the form

$$\begin{aligned} H_0 =& \frac{\omega_z}{2}\sigma_z + \triangle b^\dagger b, \\ H_1 =& \left[g_a\left(a^\dagger + \alpha^*\right)(a+\alpha) + g_b\left(b^\dagger + \beta^*\right)(b+\beta)\right. \\ &\left. + g_{ab}\left(a^\dagger + \alpha^*\right)(b+\beta) + g_{ab}\left(b^\dagger + \beta^*\right)(a+\alpha)\right]\sigma_x. \end{aligned} \tag{4}$$

In the rotating frame, $H_0 = (\omega_z/2)\,\sigma_z + \triangle b^\dagger b$, the effective Hamiltonian has approximation

$$H_E = g\left(\alpha^* b\sigma^+ + \alpha b^\dagger \sigma^-\right), \tag{5}$$

setting $g_{ab} = g$, $\sigma^+ = |e\rangle\langle g|$, and $\sigma^- = |g\rangle\langle e|$. Note that as long as the first-order magnetic field gradient is small, we can safely neglect its effects thereby validating H_E (see Appendix A1).

The mass of the resonator is approximately 5×10^{-18} kg and the zero-point fluctuation a_0 is of order 10^{-13} m [17]. The second-order magnetic field gradient is then of order 10^{14}-10^{15} T/m, corresponding to coupling $g/2\pi \sim$ 1-10 Hz [38]. Here we choose a coupling strength of $g/2\pi = 5$ Hz. From the Zeemann effect, the energy associated with the magnetic splitting of the NV center under an external magnetic field B_{ext} is $\omega_z = 2 \times 10^6 g$. The mode frequencies of the MO are set at $\omega_a = 4 \times 10^6 g$ and $\omega_b = 6 \times 10^6 g$. The driving strength is $\Omega_1 = 2.5 \times 10^5 g$ with frequency $\omega_L = \omega_a$, and the dissipation of the oscillator mode a is $\gamma_1 = 5g$ [28]. We obtain $|\alpha| = \Omega_1/\gamma_1 = 50000$. Thus, the effective coupling strength $|\alpha g|/2\pi$ is 250 kHz, which is much larger than both the mechanical decay and the NV center dephasing rate. As the external driving force has a large detuning for mode b, the driving strength for mode b is very weak and the effect of heating caused by coherent driving is negligible. Therefore, this heating can be safely neglected [32, 33]. Moreover, we can adjust the Duffing constant to suppress the nonlinearity (see Appendix A2) [41].

Furthermore, if there are many NV centers at the end of the MO, the effective interaction between the MO and NV centers increases by $\sqrt{N}$, where N is the number of NV centers [42]. Following the above steps, we derive an effective Hamiltonian

$$H_{NE} = g\left(\alpha^* d J^+ + \alpha d^\dagger J^-\right), \tag{6}$$

where $J^+ = \sum_{i=1}^N \sigma_i^+$ and the interaction among the NV centers has been neglected. From an analysis of this system, the interaction time decreases to $t/\sqrt{N}$ and the fidelity of the state rises.

2 Entanglement and state transfer

The basic requirement in quantum information processing is entanglement and state transfer between the NV center and the MO. In this section, we discuss both aspects for the hybrid system of NV center and diamond MO.

We assume that the MO is cooled to near the ground state and the NV center is in the state $|e\rangle$. We neglect initially the effects of decoherence. From eq. (5), the system evolves as:

$$|\psi(t)\rangle = -\sin(g|\alpha|t)\,|1,g\rangle + \cos(g|\alpha|t)\,|0,e\rangle, \tag{7}$$

where $|n,g\rangle$ ($|n,e\rangle$) represents the system state with the MO in the Fock state $|n\rangle$ and NV center in the ground (excited) state, respectively.

From the wave function eq. (7), we see that at time $t = \pi/4g|\alpha|$, entanglement between the NV center and MO is maximal. The entanglement of this system can be measured through negativity, which is defined as $N(\rho) = \left(\left\|\rho^{T_A}\right\| - 1\right)/2$ [43,44], where the partial transformed density matrix $\boldsymbol{\rho}^{T_A}$ has elements $\rho^{T_A}_{m\mu,n\nu} = \rho_{n\mu,m\nu}$ and the norm of the trace $\left\|\rho^{T_A}\right\| = \mathrm{tr}\sqrt{\boldsymbol{\rho}^{T_A\dagger}\boldsymbol{\rho}^{T_A}}$, which corresponds to the sum of the absolute value of eigenvalues of ρ^{T_A}. In this circumstance, negativity becomes $N(\rho) = |\sin(2g|\alpha|t)|/2$. The maximal value of $N(\rho)$ is $1/2$, corresponding to maximal entanglement.

The Jaynes-Cummings Hamiltonian eq. (5) can also be used to describe quantum-state transfer between the NV center and the MO. When the magnetic field is turned on, the interaction between the MO and NV center is established resulting in an energy exchange between MO and NV center. We see that at $t = \pi/2g|\alpha|$, its product state is excited from $|0,e\rangle$ to $|1,g\rangle$, specifically, the energy of excitation passes from the NV center to the MO. Meanwhile, the state entanglement decreases to zero corresponding to the minimal value of $N(\rho)$.

In the experiment, the effect of the environment must be considered. The state of the system is usually in a mixed state, expressed by density matrix $\boldsymbol{\rho}(t)$. We use the following master equation to describe the evolution of the density matrix

$$\begin{aligned} \dot{\rho}(t) =& -\mathrm{i}\left[H_E, \boldsymbol{\rho}(t)\right] + \frac{\gamma_2}{2}\left(\overline{n}_T + 1\right) L[b]\,\boldsymbol{\rho}(t) \\ &+ \frac{\gamma_2}{2}\overline{n}_T L\left[b^\dagger\right]\boldsymbol{\rho}(t) + \frac{d}{2}L\left[\sigma^z\right]\boldsymbol{\rho}(t), \end{aligned} \tag{8}$$

where γ_2 and d denote the dissipation rate of the MO and dephasing rate of the NV center, respectively, and $L[o]\rho = 2o\rho o^\dagger - o^\dagger o\rho - \rho o^\dagger o$. The initial MO state is a thermal state and has the form $\rho_0 = \sum_{n=0}^\infty p_n |n\rangle\langle n|$ with $p_n = \langle n\rangle^n/(1+\langle n\rangle)^{n+1}$ with $\langle n\rangle = \langle b^\dagger b\rangle$, the mean thermal phonon

number of MO. Here, we suppose MO has been cooled near the ground state. The initial state of the system is $\rho(0) = |e\rangle\langle e| \otimes \rho_0$ and the space we choose is $\{|g\rangle, |e\rangle\} \otimes \{|n\rangle\}_{n=0}^{n_{\max}}$, with upper cutoff of $n_{\max} = 20$. The dissipation rate of the MO is set to $\gamma_2 = 5g$ and the dephasing rate of the NV center to $d = 50g$. Neglecting the spontaneous decay rate of the NV center, we put this system in a low temperature environment with $\overline{n}_T = 20$, which corresponds to a temperature of around $T \simeq 10$ mK.

Once the interaction begins, entanglement occurs. Here, we explore entanglement of the system using negativity, which can be read from Figure 2. The red line in Figure 2(a) depicts the negativity of a pure state and the values of negativity are a monotonic function of entanglement. The maximal and minimal values are 1/2 and 0 corresponding to a state of maximal entanglement and the product state, respectively. However, with the influence of thermal noise of the MO, entanglement can disappear. From the plot of negativity against thermal noise (black dashed line in Figure 2(a)), we see that its maximal value falls below 1/2 and decreases with increasing thermal phonon number (see Figure 2(b)). This is because the state evolves into a mixed state due to the thermal phonon, and the components of the target state in density matrix decrease with increasing thermal phonon number.

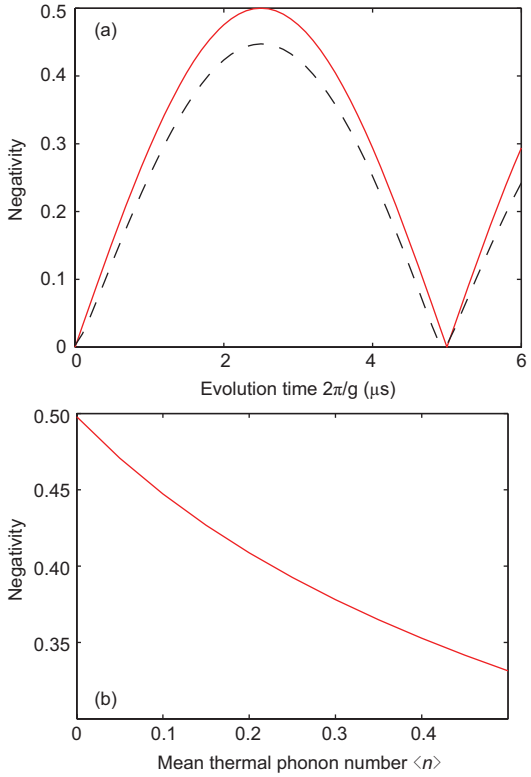

Figure 2 (Color online) Entanglement between the NV center and the MO. (a) Evolution of entanglement for pure state (red line) and actual experiment (black line) with thermal phonon number $\langle n\rangle = 0.1$; (b) negativity for maximal entanglement against the mean phonon number of the MO. The coupling strength is $g/2\pi = 5$ Hz, the driving strength is $\Omega/g = 2.5 \times 10^6$, and the dissipation rate of MO and dephasing rate of the NV center are $\gamma_2/g = 5$ and $d/g = 50$, respectively.

The fidelity is of course the essential parameter in quantum information processing, and here we investigate the fidelity of maximal entanglement state and product state. We define the fidelity between a pure target state $|\psi(t)\rangle$ and mixed state $\boldsymbol{\rho}(t)$ as $F = \sqrt{\langle\psi(t)|\boldsymbol{\rho}(t)|\psi(t)\rangle}$. That is, the fidelity is equal to the square root of the overlap between $|\psi(t)\rangle$ and $\boldsymbol{\rho}(t)$. Fidelity decays with time because of dissipation, the rate of dephasing, and thermal noise. Figure 3 presents plots of the fidelity for the maximal entanglement (a) and state transfer (b) comparing the results under different thermal noise and driving strengths. As thermal phonons can couple to other non-relevant states in the density matrix, fidelity decays with increasing thermal mean photon number. If we increase the driving strength, the effective coupling between the NV centers and the MO are enhanced, resulting in a decrease in operation time for both entanglement generation and state transfer, which may cause damage from thermal noise. From Figure 3, the influence of thermal noise decreases with increasing driving strength.

As for the interaction between the MO and the ensemble of NV centers, at $t = 0$, we assume that there are $N - 1$ NV

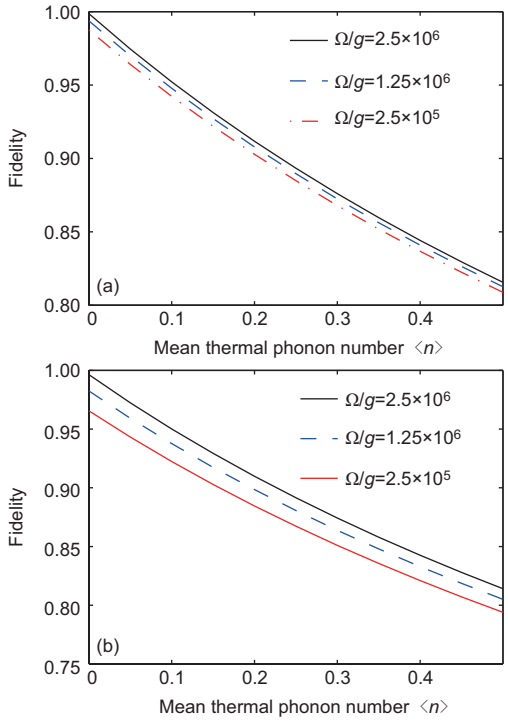

Figure 3 (Color online) Fidelity of maximal entanglement (a) and quantum state transfer (b). We give the relationship between fidelity for two operating settings and thermal noise and compare these results for different driving strengths. The dissipation rate for the MO and the rate of dephasing for the NV center are $\gamma_2/g = 5$ and $d/g = 50$, respectively.

centers in the ground state. Under the effective Hamiltonian, the evolution of the state is

$$|\psi(t)\rangle = -\sin\left(g|\alpha|\sqrt{N}t\right)|0,N\rangle + \cos\left(g|\alpha|\sqrt{N}t\right)|1,N-1\rangle, \tag{9}$$

where $|0,N\rangle$ ($|1,N-1\rangle$) denotes N ($N-1$) NV centers in the ground state and a 0 (1) photon excitation of the MO, respectively. From this wave function, we see that at $t = \pi/\left(4g|\alpha|\sqrt{N}\right)$, maximal entanglement can be achieved and at $t = \pi/\left(2g|\alpha|\sqrt{N}\right)$, the state transfer can be realized. In a low-temperature experiment, individual relaxation processes can be ignored and only dephasing of the intrinsic spin and phonon dissipation is considered. The dynamics of the system can be given by the master equation [31]

$$\dot{\rho}_N = -\mathrm{i}\left[H_E,\rho_N\right] + \frac{\gamma_2}{2}\left(\overline{n}_T+1\right)L\left[b\right]\rho_N + \frac{\gamma_2}{2}\overline{n}_T L\left[b^\dagger\right]\rho_N + \frac{d}{2}\sum_i L\left[\sigma_i^z\right]\rho_N, \tag{10}$$

where $\overline{n}_T = 20$, $d = 50g$ and $\gamma = 5g$. Because the probability of interaction between the ensemble of NV centers and the MO is high, the effective coupling strength has been enhanced, and therefore the rate of achieving the operation is fast, leading directly to an increase in fidelity. Nevertheless, more noise has been introduced into the ensemble of NV centers compared with the single NV center and decreases fidelity. The competition between the two factors leads to a compromise in fidelity for the two operations. Considering that the operation time to generate maximal entanglement is shorter, the acceleration by the NV-center ensemble is not obvious with a small number of NV centers. At the beginning, this results in a decrease in fidelity for maximal entanglement when the effect of noise plays a more important role. Later, as the effect of acceleration by the ensemble of NV centers is more obvious, that is, more NV centers are introduced, the enhanced effective coupling strength plays the leading role, producing higher fidelity (see Figure 4(a)). However, for state transfer (Figure 4(b)), the acceleration resulting from the ensemble NV centers is more obvious than the deceleration caused by noise at all times and thus, the fidelity is a monotonic function of the number of NV centers.

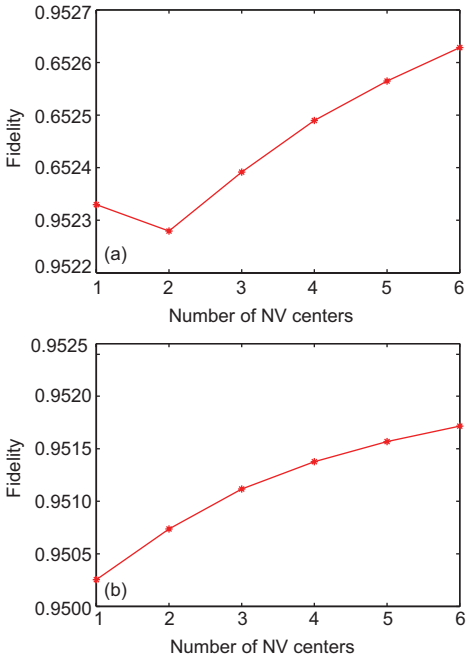

Figure 4 (Color online) Fidelity of quantum-state transfer between the ensemble of NV centers and the MO. Dependence of fidelity for maximal entanglement (a) and quantum state transfer (b) is on the number of NV centers . The thermal phonon number is $\langle n\rangle = 0.1$, the coupling strength is $\Omega/g = 2.5\times10^6$, and the dissipation rate of MO and dephasing rate of NV center are $\gamma_2/g = 5$ and $d/g = 50$, respectively.

3 Two-mode squeezing of mechanical oscillator

In addition, the second-order interaction can be applied to realize two-mode squeezing. Keeping the design and taking an extra mode c into consideration, we assume $\omega_a - \omega_c = \omega_b - \omega_a$. Mode a resonates with the external driver, and with this system, two-mode squeezing is produced. In the rotating frame, $H'_{10} = \omega_a a^\dagger a + \omega_a b^\dagger b + \omega_a c^\dagger c$, the Hamiltonian for the three-mode system is the form

$$\begin{aligned} H_{S0} =& \frac{\omega_z}{2}\sigma_z + \triangle b^\dagger b - \triangle c^\dagger c + \frac{\Omega_1}{2}\left(a+a^\dagger\right) \\ &+ \frac{\Omega_2}{2}\left(b+b^\dagger\right) + \frac{\Omega_3}{2}\left(c+c^\dagger\right), \\ H_{S1} =& \left[g_a a^\dagger a + g_b b^\dagger b + g_c c^\dagger c + g_{ab}\left(a^\dagger b + b^\dagger a\right)\right. \\ &\left. + g_{ac}\left(a^\dagger c + c^\dagger a\right) + g_{bc}\left(b^\dagger c + c^\dagger b\right)\right]\sigma_x, \end{aligned} \tag{11}$$

where $\triangle = \omega_b - \omega_a = \omega_a - \omega_c \neq \omega_z$, $a\left(a^\dagger\right)$, and $b\left(b^\dagger\right), c\left(c^\dagger\right)$ represent the annihilation (creation) operators for the three-phonon modes, respectively, of the oscillator, Ω_1 (Ω_2, Ω_3) is the driving strength applied to mode a (b, c) with frequency $\omega_L = \omega_a$, and $g_a, g_b, g_c, g_{ab}, g_{ac}, g_{bc}$ are the coupling strengths associated with the second-order magnetic field gradient. Initially, with the magnetic field absent, we drive the MO into the steady state. At steady state, the MO moves coherently undergoing transformations $a \to a+\alpha$, $b \to b+\beta$, and $c \to c+\zeta$, where α, β, and ζ are the amplitude coherent states. Similarly as in eq. (3), we obtain $\alpha = -\mathrm{i}\Omega_1/\gamma_1, \beta \simeq -\Omega_2/2\triangle$, and $\zeta \simeq \Omega_3/2\triangle$, where $\alpha \gg \beta, \zeta$. We then turn the magnetic field on and the NV centers and the MO begin to interact with each other immediately. In the rotating frame, $H'_{20} = (\omega_z/2)\sigma_z + \triangle b^\dagger b - \triangle c^\dagger c$. Neglecting high frequency

and small terms, we have

$$H_{SI} = g\left(\alpha^* b\sigma^+ e^{i\omega t} + \alpha b^\dagger \sigma^- e^{-i\omega t} + \alpha^* c^\dagger \sigma^+ e^{i\omega t} + \alpha c\sigma^- e^{-i\omega t}\right), \quad (12)$$

where $\omega = \omega_z - \triangle$ and $g_{ab} = g_{ac} = g$. In the limit $\alpha g \ll \omega$, we eliminate adiabatically the NV center [45], and obtain the effective squeezing Hamiltonian

$$H_S = \eta\left(b^\dagger b + c^\dagger c + bc + c^\dagger b^\dagger\right), \quad (13)$$

where $\eta = |\alpha|^2 g^2/\omega$, and we initially set the NV center in the excited state. As mentioned before, $2\pi|\alpha|/g = 10000$ and $\omega/g = 10^6$; therefore, we get $\eta/g = 2500$. Assuming that the initial mechanical state $|\psi(0)\rangle_S$ is the vacuum, we apply this interaction to the initial state and find

$$|\psi(t)\rangle_S = \exp\left[-i\eta\left(b^\dagger b + c^\dagger c + bc + c^\dagger b^\dagger\right)t\right]|\psi(0)\rangle_S. \quad (14)$$

We define the collective creation and annihilation operators as $d^\dagger = \left(b^\dagger + e^{i\delta}c^\dagger\right)/\sqrt{2}$ and $d = \left(b + e^{-i\delta}c\right)/\sqrt{2}$, with δ the phase difference of two modes. Based on the collective operator, the in-phase and in-quadrature components are given by $d_1 = \left(d + d^\dagger\right)/2$ and $d_2 = \left(d - d^\dagger\right)/2i$, respectively [40]. We analyze here the collective mode d_1 but the collective mode d_2 can be analyzed in the same way. The variance of d_1 in the two-mode squeezed vacuum is

$$\langle d_1^2\rangle = \frac{1 + 2(1 - \cos(\delta))\xi^2 - 2\sin(\delta)\xi}{4}, \quad (15)$$

where we denote $\xi = \eta t$. At space $(0, 2\pi)$, we see at $\xi = \sin(\delta)/[2 - 2\cos(\delta)]$, the squeezing is

$$\langle d_1^2\rangle_{\min} = \frac{1 - \cos(\delta)}{8}. \quad (16)$$

From this result, we see that the minimal value of $\langle d_1^2\rangle$ depends on δ. If we choose $\delta = \pi/2$, $\langle d_1^2\rangle = 1/8$, squeezing is accomplished.

In experiment, the dissipation of the modes needs to be taken into account. Assuming the mechanical modes have been cooled to nearly the ground state, the evolution of the state is given by the master equation

$$\dot{\rho}_S(t) = -i[H_S, \rho_S(t)] + \frac{\gamma_2}{2}(\bar{n}_T + 1)L[b]\rho_S(t) + \frac{\gamma_2}{2}\bar{n}_T L[b]\rho_S(t) + \frac{\gamma_3}{2}(\bar{n}_T + 1)L[c]\rho_S(t) + \frac{\gamma_3}{2}\bar{n}_T L[c]\rho_S(t), \quad (17)$$

where $L[o]\rho = 2o\rho o^\dagger - o^\dagger o\rho - \rho o^\dagger o$, γ_2 and γ_3 are the dissipation rate for modes b and c, respectively, and the phonon is initially in the thermal state. We see that because of the collective correlation, two-mode squeezing is realized and the variance of d_1 decreases from 1/4 to the minimal value 1/8 when we choose $\delta = \pi/2$, as in Figure 5(a). However, the correlation disappears with thermal noise and hence squeezing decreases if more thermal noise is introduced. Squeezing finally disappears when the thermal phonon number reaches 0.5 in our model as seen in Figure 5(a). The minimal value for the variance of d_1 increases linearly with the number of thermal phonons. The corresponding rate is independent of the decay rate of the MO and the driving strength, and therefore, we find that $\partial\langle d_1^2\rangle_{\min}/\partial\langle n\rangle = k$, with $k \simeq 0.25$ for this system (Figure 5(b)).

4 Discussion and conclusion

In conclusion, we have proposed a scheme to realize strong coupling between the MO and the NV centers of diamond via the second-order magnetic field gradient. We have shown that the effective coupling can be greatly enhanced by coherently

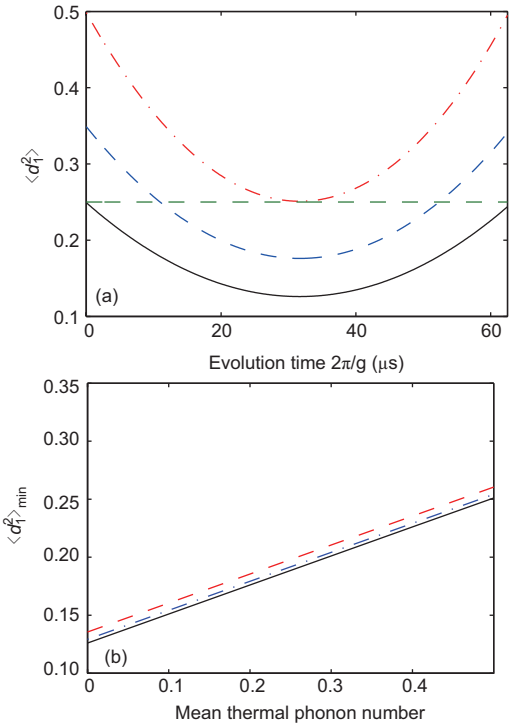

Figure 5 (Color online) Squeezing of the collective mode d_1. (a) Dynamics of $\langle d_1^2\rangle$ with $\langle n\rangle = 0, 0.2, 0.5$. The green dash line marks the critical value 1/4. The coupling strength is $g/2\pi = 5$ Hz, the driving strength is $\Omega/g = 2.5\times10^6$, and the dissipation rate for the MO is $\gamma_2/g = \gamma_3/g = 5$; (b) relationship between the minimal value of $\langle d_1^2\rangle$ and thermal phonon number of MO under three different conditions: for the black solid line, the driving strength is $\Omega/g = 2.5\times10^6$, the dissipation rate of MO is $\gamma_2/g = \gamma_3/g = 5$; for the red dashed line, the driving strength is $\Omega/g = 2.5\times10^6$, the dissipation rate of MO is $\gamma_2/g = \gamma_3/g = 50$; for the blue dot-dash line, the driving strength is $\Omega/g = 1.25\times10^6$, the dissipation rate of MO is $\gamma_2/g = \gamma_3/g = 5$. The dephasing rate of the NV center is $d/g = 50$ for both graphs.

driving the MO. We also discussed the coupling between the NV-center ensemble and the MO. Thermal noise and dissipation for both the MO and the NV centers were discussed. Based on the effective coupling, we discussed applications on quantum state transfer and entanglement generation. We found that the quantum state transfer and entanglement generation could be realized with high quality for the present experimental conditions. We also discussed how to generate two-mode squeezing for the MO via couplings to the NV centers and the external driving force. The effect of thermal noise on squeezing has been simulated. Squeezing may appear even with a non-zero thermal phonon number. We hope that our study stimulates further experimental research on the applications of the second-order magnetic field gradient in hybrid quantum systems.

This work was supported by the National Natural Science Foundation of China (Grant Nos. 61435007, 11175094, 91221205), and the National Basic Research Program of China (Grant No. 2015CB921002).

1 M. Aspelmeyer, T. J. Kippenberg, and F. Marquardt, Rev. Mod. Phys. **86**, 1391 (2014).
2 Z. Q. Yin, A. A. Geraci, and T. Li, Int. J. Mod. Phys. B **27**, 1330018 (2013).
3 Y. D. Wang, and A. A. Clerk, Phys. Rev. Lett. **108**, 153603 (2012).
4 L. Tian, Phys. Rev. Lett. **108**, 153604 (2012).
5 R. W. Andrews, R. W. Peterson, T. P. Purdy, K. Cicak, R. W. Simmonds, C. A. Regal, and K. W. Lehnert, Nat. Phys. **10**, 321 (2014).
6 Z. Yin, W. L. Yang, L. Sun, and L. M. Duan, Phys. Rev. A **91**, 012333 (2015).
7 Y. C. Liu, Y. F. Xiao, X. Luan, and C. W. Wong, Sci. China-Phys. Mech. Astron. **58**, 050305 (2015).
8 Y. Yan, W. J. Gu, and G. X. Li, Sci. China-Phys. Mech. Astron. **58**, 050306 (2015).
9 G. Z. Wang, M. M. Zhao, J. Y. Ma, G. Y. Li, Y. Chen, X. S. Jiang, and M. Xiao, Sci. China-Phys. Mech. Astron. **58**, 1 (2015).
10 M. Gao, F. C. Lei, C. G. Du, and G. L. Long, Sci. China-Phys. Mech. Astron. **59**, 610301 (2016).
11 A. M. Flatae, M. Burresi, H. Zeng, S. Nocentini, S. Wiegele, C. Parmeggiani, H. Kalt, and D. Wiersma, Light Sci Appl **4**, e282 (2015).
12 I. Wilson-Rae, N. Nooshi, W. Zwerger, and T. J. Kippenberg, Phys. Rev. Lett. **99**, 093901 (2007).
13 Y. S. Park, and H. Wang, Nat. Phys. **5**, 489 (2009).
14 Y. C. Liu, R. S. Liu, C. H. Dong, Y. Li, Q. Gong, and Y. F. Xiao, Phys. Rev. A **91**, 013824 (2015).
15 S. M. Meenehan, J. D. Cohen, G. S. MacCabe, F. Marsili, M. D. Shaw, and O. Painter, Phys. Rev. X **5**, 041002 (2015).
16 D. Rugar, R. Budakian, H. J. Mamin, and B. W. Chui, Nature **430**, 329 (2004).
17 P. Rabl, P. Cappellaro, M. V. G. Dutt, L. Jiang, J. R. Maze, and M. D. Lukin, Phys. Rev. B **79**, 041302 (2009).
18 Z. Y. Xu, Y. M. Hu, W. L. Yang, M. Feng, and J. F. Du, Phys. Rev. A **80**, 022335 (2009).
19 L. Zhou, L. F. Wei, M. Gao, and X. Wang, Phys. Rev. A **81**, 042323 (2010).
20 D. Gevaux, Nat. Phys. **6**, 8 (2010).
21 P. B. Li, Y. C. Liu, S. Y. Gao, Z. L. Xiang, P. Rabl, Y. F. Xiao, and F. L. Li, Phys. Rev. Appl. **4**, 044003 (2015).
22 P. B. Li, Z. L. Xiang, P. Rabl, and F. Nori, Phys. Rev. Lett. **117**, 015502 (2016).
23 A. D. OConnell, M. Hofheinz, M. Ansmann, R. C. Bialczak, M. Lenander, E. Lucero, M. Neeley, D. Sank, H. Wang, M. Weides, J. Wenner, J. M. Martinis, and A. N. Cleland, Nature **464**, 697 (2010).
24 O. Arcizet, V. Jacques, A. Siria, P. Poncharal, P. Vincent, and S. Seidelin, Nat. Phys. **7**, 879 (2011).
25 S. Kolkowitz, A. C. Bleszynski Jayich, Q. P. Unterreithmeier, S. D. Bennett, P. Rabl, J. G. E. Harris, and M. D. Lukin, Science **335**, 1603 (2012).
26 L. P. Neukirch, E. von Haartman, J. M. Rosenholm, and A. Nick Vamivakas, Nat. Photon **9**, 653 (2015).
27 T. M. Hoang, J. Ahn, J. Bang, and T. Li, Nat. Commun. **7**, 12250 (2016).
28 Y. Tao, J. M. Boss, B. A. Moores, and C. L. Degen, Nat. Commun. **5**, 3638 (2014).
29 D. A. Golter, T. Oo, M. Amezcua, K. A. Stewart, and H. Wang, Phys. Rev. Lett. **116**, 143602 (2016).
30 M. W. Doherty, N. B. Manson, P. Delaney, F. Jelezko, J. Wrachtrup, and L. C. L. Hollenberg, Phys. Rep. **528**, 1 (2013).
31 S. D. Bennett, N. Y. Yao, J. Otterbach, P. Zoller, P. Rabl, and M. D. Lukin, Phys. Rev. Lett. **110**, 156402 (2013).
32 J. Teissier, A. Barfuss, P. Appel, E. Neu, and P. Maletinsky, Phys. Rev. Lett. **113**, 020503 (2014).
33 A. Barfuss, J. Teissier, E. Neu, A. Nunnenkamp, and P. Maletinsky, Nat. Phys. **11**, 820 (2015).
34 Z. Q. Yin, N. Zhao, and T. C. Li, Sci. China-Phys. Mech. Astron. **58**, 050303 (2015).
35 T. C. Li, and Z. Q. Yin, Sci. Bull. **61**, 163 (2016).
36 Z. Yin, T. Li, X. Zhang, and L. M. Duan, Phys. Rev. A **88**, 033614 (2013).
37 W. Ge, and M. Bhattacharya, New J. Phys. **18**, 103002 (2016).
38 Y. Ma, Z. Yin, P. Huang, W. L. Yang, and J. Du, Phys. Rev. A **94**, 053836 (2016).
39 Z. Yin, Phys. Rev. A **80**, 033821 (2009).
40 M. O. Scully, and M. S. Zubairy, *Quantum Optics* (Cambridge University Press, Cambridge, 2012).
41 P. Huang, J. Zhou, L. Zhang, D. Hou, S. Lin, W. Deng, C. Meng, C. Duan, C. Ju, X. Zheng, F. Xue, and J. Du, Nat. Commun. **7**, 11517 (2016).
42 Z. Yin, and F. Li, Phys. Rev. A **75**, 012324 (2007).
43 A. Peres, Phys. Rev. Lett. **77**, 3264 (1996).
44 G. Vidal, and R. F. Werner, Phys. Rev. A **65**, 032314 (2002).
45 D. F. James, and J. Jerke, Can. J. Phys. **85**, 625 (2007).

Appendix A1 First-order magnetic field gradient effects

We briefly discuss the first-order magnetic field gradient effects. If both the first- and second-order magnetic field gradient are considered, we should add the following first-order magnetic field gradient induced coupling terms in eq. (1)

$$H_2 = g_{1a}(a + a^\dagger)\sigma_x + g_{1b}(b + b^\dagger)\sigma_x, \tag{a1}$$

where g_{1a} (g_{1b}) is the first-order magnetic field gradient-induced coupling strength between NV centers and mechanical oscillator a (b). In the rotating frame $H_{10} = \frac{\omega_z}{2}\sigma_z + \omega_a(a^\dagger a + b^\dagger b)$, these first-order coupling terms become

$$\begin{aligned} H_2' = {} & g_{1a}(a\mathrm{e}^{-\mathrm{i}\omega_a t} + a^\dagger \mathrm{e}^{\mathrm{i}\omega_a t})(\sigma_+ \mathrm{e}^{\mathrm{i}\omega_z t} + \sigma_- \mathrm{e}^{-\mathrm{i}\omega_z \mathrm{t}}) \\ & + g_{1b}(b\mathrm{e}^{-\mathrm{i}\omega_a t} + b^\dagger \mathrm{e}^{\mathrm{i}\omega_a t})(\sigma_+ \mathrm{e}^{\mathrm{i}\omega_z t} + \sigma_- \mathrm{e}^{-\mathrm{i}\omega_z t}). \end{aligned} \tag{a2}$$

In the absence of any driving on mode a, we can neglect eq. (a2) in using the rotating wave approximation because $|\omega_a \pm \omega_z|$ is much larger than the coupling terms g_{1a} and g_{1b}. Even if the a is coherently driven (with the steady state amplitude α), as long as $\alpha g_{1a} \ll \omega_L$, the rotating wave approximation is still valid. In our scheme, α is chosen around 50000. To neglect H_2', the g_{1a} should be much less than $|\omega_a - \omega_z|/\alpha = 200 \times 2\pi$ Hz. Therefore, as long as the first-order magnetic field gradient is small enough, we can neglect its effects.

Appendix A2 Nonlinearity in our model

When the amplitude of the MO is enhanced, a cubic nonlinearity (Duffing nonlinearity) may be important. Fortunately, effects caused by cubic nonlinearity can be neglected in our model. The dynamics of the MO in our model can be modeled by a simplified driven Duffing oscillator equation

$$m\ddot{x} + k_1 x + k_3 x^3 = F_{\text{drive}}\cos(\omega t), \tag{a3}$$

where m, x, k_1, and k_3 are the mass, amplitude, liner spring constant, and Duffing constant, respectively. In our system, the mass is around 5×10^{-18} kg, the amplitude of MO is about 1 nm. According to ref. [41], the Duffing constant is about 10^{14} Nm^{-3}. Hence, $k_3 x^2 \ll k_1$ and the nonlinearity can be neglected.

As for the interaction between the NV center and the MO in our model, the third-order coupling can also be neglected. We know that the bridge between the NV center and MO is the magnetic field $B(x)$, which can be expanded as:

$$\begin{aligned} B(x) =& B_0 + \frac{\mathrm{d}B(x)}{\mathrm{d}x}\Delta x + \frac{\mathrm{d}^2B(x)}{\mathrm{d}x^2}(\Delta x)^2 \\ &+ \frac{\mathrm{d}^3B(x)}{\mathrm{d}x^3}(\Delta x)^3 + \cdots . \end{aligned} \tag{a4}$$

Because the magnetic tips are arranged symmetrically, the magnetic field $B(x)$ is an even function and hence the third-order coupling vanishes.